Proceedings of The Canadian Society for Mechanical Engineering Forum 2010
CSME FORUM 2010
June 7-9, 2010, Victoria, British Columbia, Canada

Reachable Workspace Comparison of Revolute Pair Jointed and Algebraic Screw Pair Jointed Kinematic Chains

JAMES D. ROBINSON
Department of Mechanical and Aerospace Engineering
Carleton University
Ottawa, Ontario, Canada, K1S 5B6
jrobins7@connect.carleton.ca

M. JOHN D. HAYES
Department of Mechanical and Aerospace Engineering
Carleton University
Ottawa, Ontario, Canada, K1S 5B6
jhayes@mae.carleton.ca

Abstract: *A new kinematic pair called an algebraic screw pair, or A-pair, is introduced that utilizes the self-motions inherent to a specific configuration of Griffis-Duffy platform. Using the A-pair as a joint in a hybrid parallel-serial kinematic chain results in a sinusoidal coupling of rotation and translation between adjacent links. The resulting linkage is termed an A-chain. This paper presents initial work towards visualizing the workspace of A-chains by considering short planar and spatial serial chains connected with two A-joints. These are called 2A-chains. An additional goal is to compare similar R- and A-chains. Preliminary work in this area is also presented.*

1 Introduction

The A-pair [1] is a novel kinematic pair which exploits the single degree of freedom (DOF) self-motion produced by a specific configuration of Griffis-Duffy platform (GDP) [2], which is a special configuration of Stewart-Gough platform (SGP). Self-motions represent situations where the end effector (EE) of the manipulator can move in an uncontrolled manner without actuator input. The rationale behind proposing this new kinematic pair, called an algebraic screw pair, or A-pair, is based on the hypothesis that replacing the revolute pairs (R-pairs) in a serial manipulator with A-pairs will enhance the rigidity of the serial arm [1]. This paper focuses on development of techniques for visualization of the workspace of A-chains with one and two joints. Quantifying the resulting difference in reachable workspace volume of similar R- and A-chains is necessary to justify the development of this new class of kinematic pair.

The reachable workspace of a manipulator is the space a reference point on the EE can reach in at least one orientation [3]. Analysis of the reachable workspace is typically approached using either numerical or analytic techniques with the former being much more abundant in literature and the later being either focused on very specific manipulators (usually short R-chains) or addressed in a general manner very similar to techniques used to find the direct kinematics of a manipulator. The numeric analysis appears to begin with Roth in 1975 [4] where the relationship between the kinematic geometry of a manipulator and its performance is examined. In 1980 and 1981 numerical algorithms for tracing the boundary surfaces of a mechanisms workspace are proposed in [5, 6].

In 1983 Yang and Lee published two companion articles [7, 8]. The first paper suggests a method for analytically determining the workspace of a manipulator which, as presented in the paper, is essentially the same as obtaining the direct kinematic equations. The paper then continues by discussing how to find holes and voids in the reachable workspace of R-chains by starting at the joint closest to the EE, looking at the workspace and then moving to the next joint and examining how the cross-section of the first workspace interacts with the joint axis to determine if any holes or voids are created. The process is then recursively applied to each successive joint until the base is reached. This technique can be used for R-chains but is not general enough to be easily adapted to A-chains. The companion paper, [8], presents an algorithm for finding the workspace boundaries, uses the cross-section of the workspace to determine its volume, and proposes several performance indices. The algorithm for the boundary determination is the basis of a method that will be discussed in more detail later. The proposed performance indices, the volume index (VI), relates the volume of the manipulator workspace to the total length of the manipulator. The VI may be a useful tool when comparing the reachable workspace of R-chains and A-chains, though it will not be the only one used.

Tsai and Soni [9] recognized that as the number of joints in an R-chain increases it becomes increasingly impractical to describe

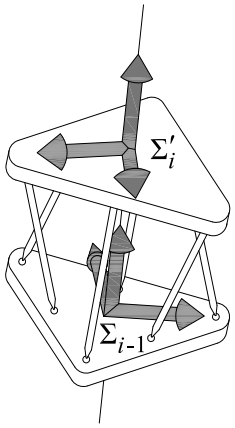

Figure 1: Midline-to-vertex GDP configuration.

the boundaries of the workspace by explicit equations. They instead describe how to find the contour of the workspace on an arbitrary plane and suggest using multiple planes to gain an understanding of the workspace as a whole. In 1986 Kumar and Patel [10] looked at issues, existing at the time, concerning the graphical represention and manipulating the workspace of a manipulator on a computer display. The technique involves representing the workspace as a series of pixels. In 2008, a similar technique is employed by Castelli, Ottaviano and Ceccarelli [11] that divides the ambient space around a manipulator into pixels and steps through the available joint angles to determine which pixels can be reached by the manipulator. The theory reported in [11] is the start point for the algorithm developed in this research, and the technique will be discussed in more detail in the next section.

In this paper the unique kinematic geometry of the A-chain is introduced. It's displacement characteristics are discussed, and relevant Denavit-Hartenberg (DH) parameters defined. An adapted Castelli algorithm [11] is proposed and applied to the visualization of the A-chain reachable workspace, and the reachable workspaces of R- and A-chains with one and two DOF are compared.

2 Kinematic Geometry of A-Chains

The A-pair comprises one particular configuration of GDP called the midline-to-vertex configuration, illustrated in Figure 1, where a leg with an anchor point on the fixed base has an anchor point on the midpoint of one of the edges of the triangle on the moving platform and vice versa, maintaining the same order of legs around the perimeter of the fixed base and moving platform. Additional constraints applied include: the fixed base and moving platform triangles are congruent equilateral triangles; and the six legs are all of a fixed length, l, equal to the height, h, of the triangles made by their anchor points (distance from the midpoint of one of the edges of the triangle to the opposite vertex on the same triangle).

When working with kinematic pairs that have a limited range of motion or, as is also the case with A-pairs, where there is a coupling of two or more DH-parameters it is necessary to identify the direction of the home position (or some other reference position) of the joint with respect to the preceding link in the kinematic chain. The A-pair has both a limited range of motion [12] and couples the joint angle with the joint offset so it is important to know which way the A-pair is attached to the preceding link.

It is necessary to decompose the joint angle into two components, one fixed and one variable. The fixed component of the joint angle, θ_f, is the angle between adjacent links when the A-pair is in the home position. The home position is when the upper an lower triangles are coincident [1, 12] (this is a theoretical position that can be reached only if self collisions are ignored). The variable component of the joint angle, θ_v, is measured relative to the home position. That is, when $\theta_v = 0$ the joint is in the home position.

With this definition the separation of the fixed base and moving platform of the A-pair is a function of θ_v and is independent of θ_f. The equation for the separation, denoted d, is:

$$d = \rho \sin\left(\frac{\theta_v}{2}\right), \tag{1}$$

where ρ is a function of the geometry of the GDP. The current work focuses on a GDP constructed such that the fixed base and moving platform are congruent equilateral triangles with each side of the triangles being of length a. The value for ρ obtained using this GDP geometry is

$$\rho = \frac{a\sqrt{6}}{3}. \tag{2}$$

Four DH-parameters are used to unambiguously describe the kinematic geometry of each link in an n-link serial chain. For link i, where $i \in 1, \ldots, n$, the DH-parameters are defined as:

- *link length*, a_i, is the length of the common normal between adjacent joint axes;
- *link twist*, α_i, is the angle between adjacent joint axes about the line defining link i;
- *joint offset*, d_i, is the offset along the joint axis of two adjacent links; and
- *joint angle*, θ_i, is the angle between adjacent links about the joint axis.

For A-pairs it is important to clarify the definitions of the joint angle and joint offset. The joint angle must be broken into two components, one fixed and one variable. The fixed component, θ_{fi}, refers the angle between adjacent links about the joint axis when the A-pair is in its home position. The variable component, θ_{vi}, is measured from the home position and it is this variable component that is used in Eqn. (1) to determine the separation of the fixed base and moving platform of the A-pair. The total joint

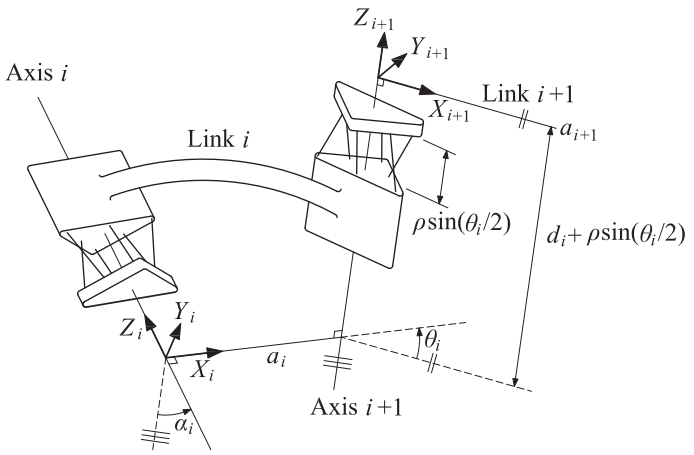

Figure 2: The DH-parameters for a link in an A-chain with appropriate coordinate systems attached.

angle is $\theta_i = \theta_{fi} + \theta_{vi}$. The coupling of translation and rotation requires that the total joint offset also be broken into fixed and variable components. When working with A-pairs the parameter d_i refers to the the fixed component, that is, the distance along the joint axis between adjacent links when the joint is in the home position ($\theta_{iv} = 0$). The variable component of the joint offset is provided by Eqn. (1). The DH-parameters of the A-chain are illustrated in Figure 2.

In addition to DH-parameters each link is assigned one reference coordinate system, and the assignment of this coordinate system depends on the two joint axes at the ends of the link. For the purposes of this description, each link i, $i = 1, \ldots, n$ describes a rigid link that lies on the common normal between axes i and $i + 1$, regardless of the actual shape of the physical link in the manipulator, which is irrelevant to the kinematic analysis. Let coordinate system i be denoted Σ_i. The origin of Σ_i located where link i intersects the joint axes i. The Z_i-axis of Σ_i points along the i^{th} joint axis, the direction is arbitrary but, with experience, is selected to ease future calculations. The X_i-axis points along the common perpendicular towards the origin of Σ_{i+1}. If the axes i and $i + 1$ intersect, the axis X_i is parallel to the normal of to the intersecting axes, the direction is again selected to ease future calculations. The Y_i-axis is assigned to complete the right-handed coordinate system. This procedure works well for intermediate links, however the base and EE coordinate systems, Σ_0 and Σ_n respectively, are often selected to ease calculations by setting as many DH-parameters to zero as possible. Figure 2 shows the placement of two adjacent coordinate systems in an A-chain.

3 Reachable Workspace Analysis

The reachable workspace of a manipulator is the space a reference point on the EE can reach in at least one orientation [3]. The algorithm that is described here (based on [11]) considers the reachable workspace literally as a structured cloud of points. The algorithm involves discretizing the ambient space around the manipulator into three dimensional elements called pixels and incrementing each joint angle in sequence by a small amount to determine which pixels are reached by the EE. The following outlines the algorithm step-by-step.

1. Determine the extreme values in each of the X, Y and Z axes that can be reached by the EE of the manipulator.

2. Select the desired resolution in each axis (the dimensions of each pixel), ΔX, ΔY and ΔZ.

3. Define two three dimensional arrays, $\mathbf{P}_{ijk}$ and $\mathbf{D}_{ijk}$, that each represent the discretized ambient space, that is each of the elements in the arrays represents one pixel of the ambient space. $\mathbf{P}_{ijk}$ is a three dimensional binary array whose elements are set equal to one if the EE of the manipulator can be placed within that pixel and zero if it cannot. $\mathbf{D}_{ijk}$ counts the number of times a particular pixel is reached by the EE as each joint of the manipulator is incremented. The elements of both matrices are initially set to zero.

4. Starting with a predetermined set of joint variables, sequentially step each joint variable by a small amount and complete the following steps for every possible combination of joint variables. The step size must be determined for each manipulator based on its design parameters and the ambient space pixel size (based on the required accuracy and time/computing power constraints).

   4.1 Determine, using the direct kinematics, the position of the EE in the ambient space.

   4.2 Determine which pixel the EE is in (*i.e.* determine the values of i, j, k in the subscript of the $\mathbf{P}_{ijk}$ and $\mathbf{D}_{ijk}$ matrices).

   4.3 Set the element of $\mathbf{P}_{ijk}$ corresponding to the reached pixel equal to one, if it is not already equal to one, to indicate that the pixel corresponding to that array element has been reached.

   4.4 Increment the element of $\mathbf{D}_{ijk}$ corresponding to the reached pixel by one to count the number of times that pixel is reached.

The geometry of the manipulator is defined using DH-parameters as well as any required joint geometry parameters such as ρ. Also defined are the variables for the ambient space surrounding the manipulator such as the maximum and minimum values in the X, Y and Z directions (X_{max}, X_{min}, *etc.*); and the resolution of the pixels in each direction: ΔX, ΔY and ΔZ. The step size (the amount that the joints are moved between each iteration) is also selected and is based on the size of the pixels and the geometry of the manipulator. At this time trial and error is used to determine the best value of the step size (too small and

the simulation takes too long to run, too large and there will be gaps in the workspace).

The array representations of the workspace, $\mathbf{P}_{ijk}$ and $\mathbf{D}_{ijk}$, are initialized based on the maximum and minimum values along each axis and the resolution specified by ΔX, ΔY and ΔZ. The elements of these two arrays are all set to zero to indicate that the corresponding pixels have not yet been reached by the EE of the manipulator.

With the geometry defined and the ambient space discretized it is now necessary to loop through all possible joint variable combinations and determine the position of the EE in each configuration. The matrices for computing the direct kinematics are obtained using the method shown in [1].

The X, Y and Z positions of the origin of the EE coordinate system are obtained from the first column of the transformation matrix from the base coordinate system to the EE coordinate system, $\mathbf{T}$ (the second, third and fourth elements of that vector respectively) and adjusted such that the position $(0, 0, 0)$ is in the centre of the ambient space. The pixel coordinates corresponding to the EE position are obtained by

$$i = \text{floor}\left(\tfrac{X-\Delta X}{\Delta X}\right),\ j = \text{floor}\left(\tfrac{Y-\Delta Y}{\Delta Y}\right),\ k = \text{floor}\left(\tfrac{Z-\Delta Z}{\Delta Z}\right),$$

where the floor() operator returns the nearest integer that is less than or equal to the value inside the brackets. These pixel coordinates correspond to an element in the discretized ambient space arrays $\mathbf{P}_{ijk}$ and $\mathbf{D}_{ijk}$ and the matrices are updated accordingly ($\mathbf{P}_{ijk}(i, j, k)$ is set equal to one to indicate that the pixel has been reached at least once and $\mathbf{D}_{ijk}(i, j, k)$ is incremented by one to count the number of times the pixel has been reached).

Once the iterations are complete the workspace has been obtained for the manipulator at the resolution defined by the size of the pixels and the joint variable step size for each iteration. The elements of $\mathbf{P}_{ijk}$ can be plotted in three dimensions to provide for an overview of the workspace or a cross section of the workspace can be plotted to look for things like voids or holes.

At the current time nothing is done with the $\mathbf{D}_{ijk}$ array, but in the future it will be used to start the investigation of the dexterity of the manipulator. It is also useful for determining an appropriate joint variable step size for the ambient space resolution. If the count of the number of times a pixel is reached is very high (especially for a simple manipulator) it may indicate that the step size is small for the given resolution and the simulation will take longer to complete than necessary. The results of the simulation are saved as a data file so that they can be kept for future use without having to re-run the simulation.

3.1 The Reachable Workspaces of Single-Joint Chains

There are infinitely many configurations of manipulator that can be constructed with different numbers of joints and different sets of parameters making it difficult to simply compare R-chains with A-chains. To gain an initial understanding of relevant issues, the current work is restricted to short chains comprising one and two joints. At this point the all joints will be limited to the range $60^\circ \leq \theta_i \leq 300^\circ$ in order to correspond to the absolute maximum range of an A-pair [12]. Self-collisions between the links of the manipulator are also being ignored at this time.

In order to show the characteristics of the A-chain workspace a very large A-pair relative to the size of the links has been used (the side of one of the sides of the triangles, a, has been set to 10). In reality the joint would likely be much smaller than the links and the shape of the workspace would not be as exaggerated. This is important to remember since at first glance the 2R- and 2A-chains bear little resemblance to one another.

Examining the workspace of chains with only one joint appears trivial, but it is important to understand how each joint in the chain works in order to fully understand and predict how a chain of multiple joints might move in space.

Figure 3 compares the reachable workspaces of a 1R-chain and a 1A-chain. The 1R-chain has the DH-parameters (the units are irrelevant): $a_1 = 10$, $\alpha_1 = 0^\circ$, and $d_1 = 6$, and the DH-parameters of the 1A-chain are: $a_1 = 10$, $\alpha_1 = 0^\circ$, $d_1 = 0$ and the fixed component of the joint angle is $\theta_{f1} = 0^\circ$. The difference in the joint offset (d_1) between the two manipulators is set so the workspaces of the manipulators will overlap.

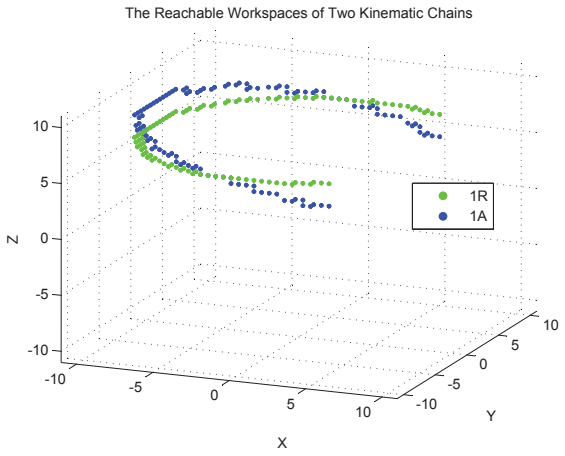

Figure 3: Plots of the reachable workspaces of a 1R-chain and a 1A-chain.

The workspace of the of the 1R-chain is a planar semi-circle while the workspace of the 1A-chain is a semi-circle when projected onto the X-Y plane, but the Z value varies according to $Z = \rho \sin(\theta_v/2)$. Near the beginning and end of the range of rotation the 1A-chain workspace is below the 1R-chain while near the middle of the range of rotation it is above.

3.2 The Reachable Workspaces of 2-Joint Chains

Comparing two-jointed chains becomes increasingly difficult because there are many more configuration possibilities. Three relatively simple cases are examined: the axes of the two joints are parallel (the workspace of the 2R-chain is planar); the joint axes

are perpendicular but not intersecting; the axes are perpendicular and intersect.

3.2.1 Parallel Axes

When a 2R-chain has parallel joint axes (and links with non-zero lengths) the reachable workspace lies on a plane. The shape of the planar workspace depends on the link lengths and available range of motion of each joint, however the reachable workspace will typically be a circular band whose thickness depends on the length of the second link and the range of rotation of the second joint.

The DH-parameters of the 2R- and 2A-chains used here are listed in Table 1. Joint offsets of six units were used in order

Table 1: DH-Parameters of the 2-jointed chains with parallel axes.

Chain/Link i	a_i	α_i	d_i	θ_{fi}	θ Range
2R-Chain					
1	10	180°	6	N/A	$60° \leq \theta_1 \leq 300°$
2	5	0°	6	N/A	$-120° \leq \theta_2 \leq 120°$
2A-Chain					
1	10	180°	0	0°	$60° \leq \theta_1 \leq 300°$
2	5	0°	0	180°	$60° \leq \theta_2 \leq 300°$

to remain consistent with the 1R-chain from the previous section and the link twist of $180°$ was used such that the plane of the reachable workspace would be on the X-Y plane at $Z = 0$. The workspace of this manipulator is illustrated in Figure 4.

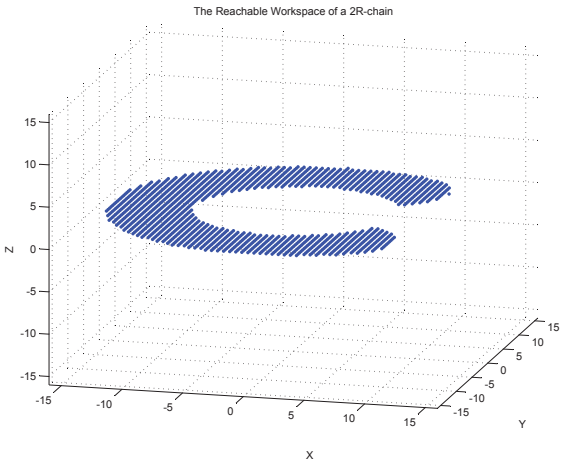

Figure 4: Plot of the reachable workspace of a 2R-chain with parallel axes.

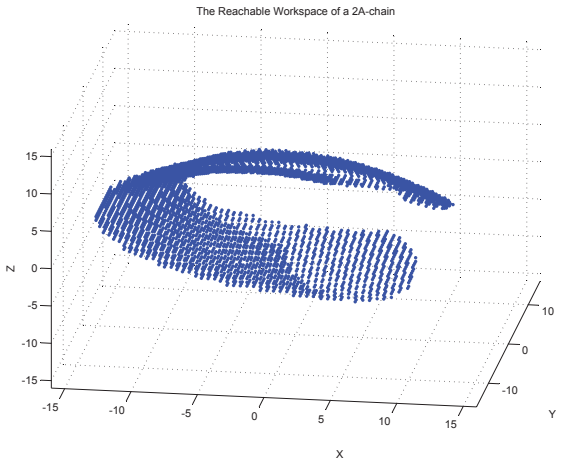

Figure 5: Plot of the reachable workspace of a 2A-chain with parallel axes.

The workspace of the 2R-chain is to be compared to a dimensionally similar 2A-chain. Because of the coupled translation and rotation the reachable workspace of the 2A-chain is no longer in the plane and is a more complex shape than that of the planar 2R-chain, as seen in Figure 5. To gain better understanding of the shape features, several cross-sections of the workspace are examined. Figure 6 shows several cross-sections of the 2A-chain reachable workspace. The cross-sections show that the 2A-chain workspace does not contain any large planar segments like the 2R-chain, suggesting that the reachable workspaces of the two types of chains have little in common.

Using the pixel representation of the ambient space around the manipulator it is possible to determine which pixels are reached by both types of manipulators, this gives some insight into the intersection of the two workspaces. It must be noted that because of the discretization of the ambient space the same pixel may be activated, but in reality the same exact point in space has not been reached. Figure 7 shows the intersection of the workspaces. The intersection appears to be segments of a plane, but in reality it is likely curves on the plane. This is similar to the point intersection in Figure 3 appearing as three pixels because of the coarse discretization of the ambient space.

3.2.2 Non-Intersecting Perpendicular Axes

In this configuration the 2R-chain reachable workspace differs from the previous configurations in that it is no longer planar. The DH-parameters of the two 2R- and 2A-chains with non-intersecting perpendicular axes are listed in Table 2. For the 2R-chain joint offsets of $d_i = 8$ were used to put the two workspaces in the same region of the ambient space. The pixel resolution is 0.5 units.

The reachable workspace of the 2R-chain is the toroidal sec-

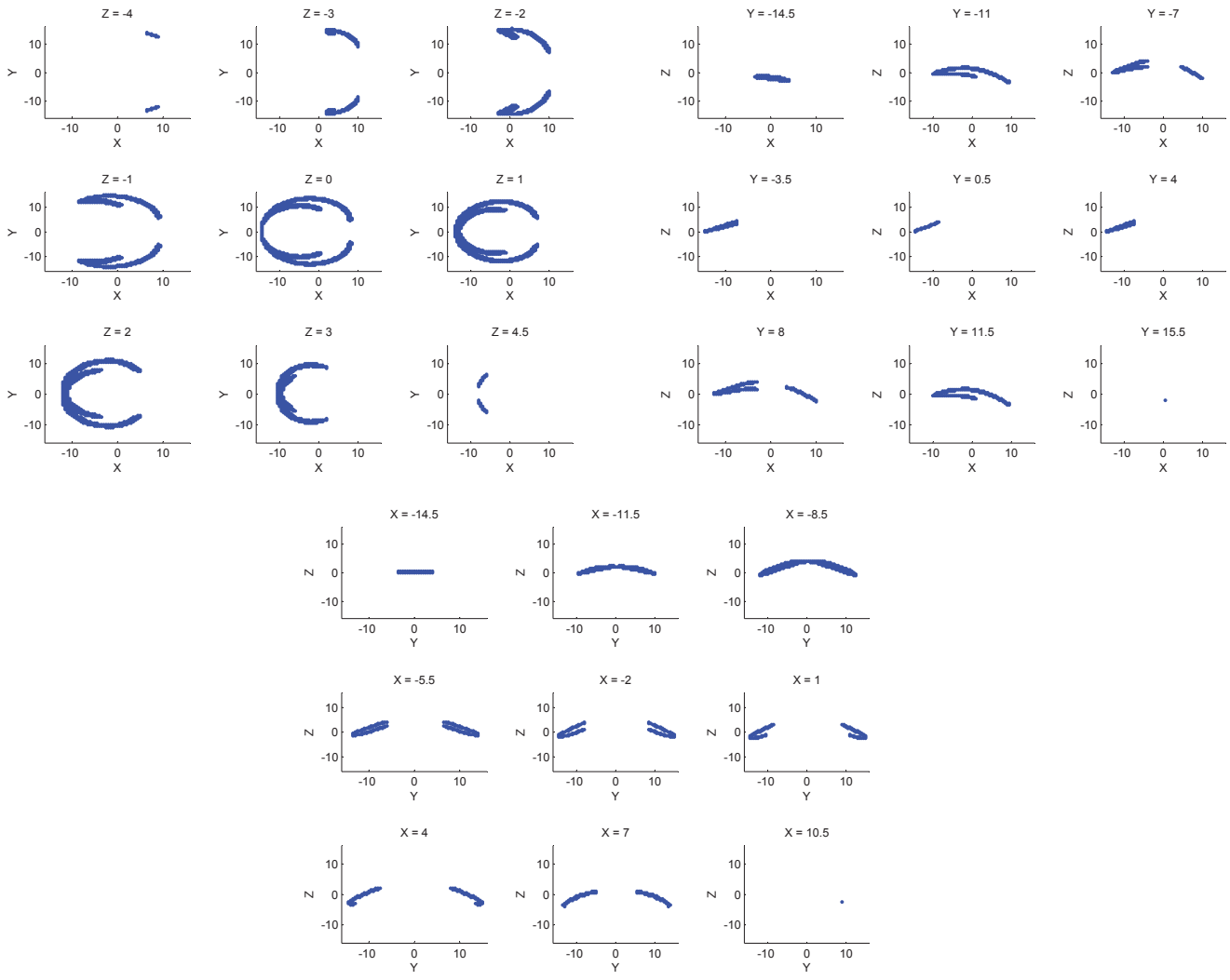

Figure 6: Cross-sections of the reachable workspace of a 2A-chain with parallel axes.

Table 2: DH-Parameters of the 2-jointed chains with non-intersecting perpendicular axes.

Chain/Link i	a_i	α_i	d_i	θ_{fi}	θ Range
2R-Chain					
1	10	90°	8	N/A	$60° \leq \theta_1 \leq 300°$
2	5	0°	8	N/A	$-120° \leq \theta_2 \leq 120°$
2A-Chain					
1	10	90°	0	0°	$60° \leq \theta_1 \leq 300°$
2	5	0°	0	180°	$60° \leq \theta_2 \leq 300°$

tion with a plane of symmetry parallel to the X-Y plane at $Z = 8$, seen in in Figure 8. At first glance the reachable workspace of the geometrically similar 2A-chain (shown in Figure 9) appears to be similar to that of the 2R-chain, but the 2A-chain workspace has no plane of symmetry. An estimate of the intersection of the reachable workspaces of the two manipulators can be obtained by determining which pixels in the ambient space are reached by both the 2R- and 2A-chain.

Figure 10 reveals the intersection of the two workspaces. The scatter plot of the common pixels shows that the two workspaces intersect in a planar semi-circle. Some of the additional pixels that the two workspaces have in common are artifacts of the coarseness of the pixels resolution. This shows that the 2A-chain can only reach a somewhat small number of the same points as a 2R-chain. Regardless, the study so far has only considered the ability of the A-chains to match geometrically equivalent R-chains and not any quantitative comparisons (*i.e.* workspace area, *etc.*).

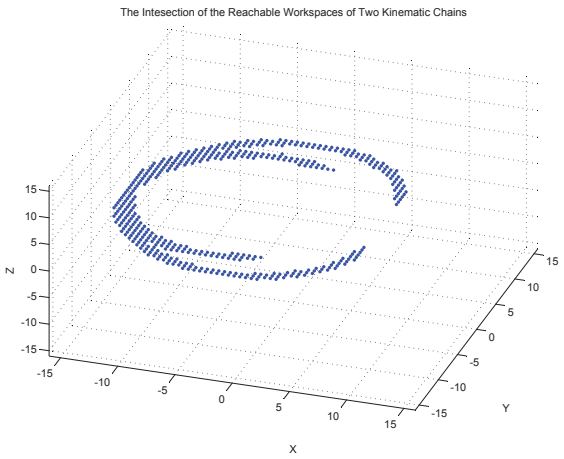

Figure 7: Plot of the intersection of the 2R-chain and 2A-chain reachable workspaces for 2-jointed chains with parallel axes.

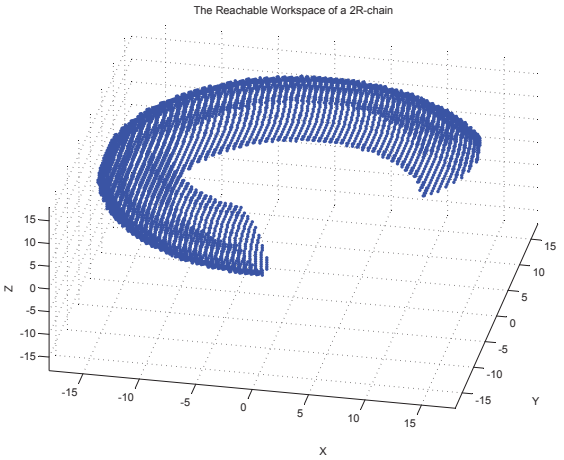

Figure 8: Plot of the reachable workspace of a 2R-chain with non-intersecting perpendicular axes.

3.2.3 Intersecting Perpendicular Axes

The DH-parameters of the two chains are provided in Table 3. The joint offset of the second joint, $d_2 = 18$, was selected to account for the length of the first link (different from a_1 for intersecting joint axes) that is 10 units long and also to account for the inherent joint offset of A-pairs, approximately 8 units. The pixels shared by the two workspaces are illustrated in Figure 11. The intersection appears to be a portion of the band that is the workspace of the 2R-chain, though with a finer pixel resolution the intersection may reduce to a planar semi-circle.

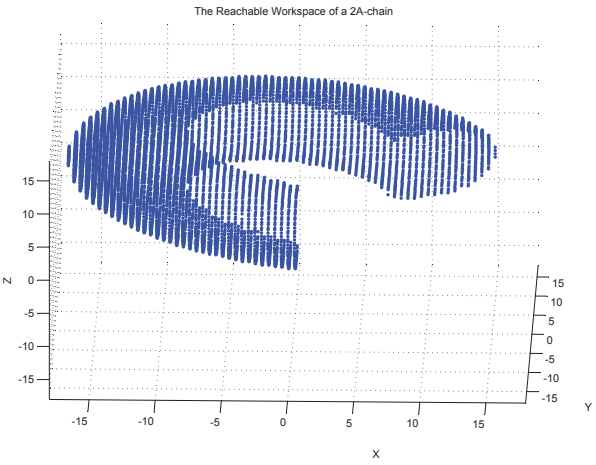

Figure 9: Plot of the reachable workspace of a 2A-chain with non-intersecting perpendicular axes.

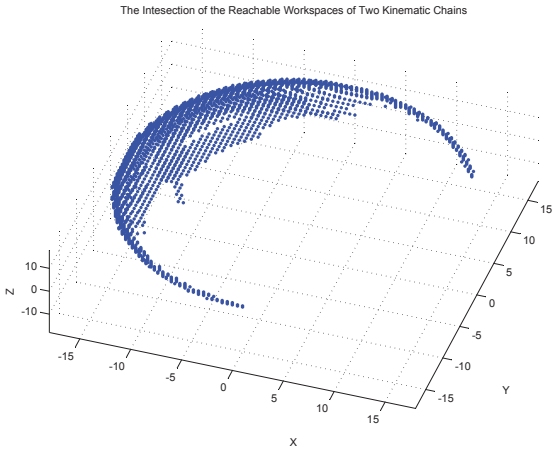

Figure 10: Plot of the intersection of the 2R-chain and 2A-chain reachable workspaces for 2-jointed chains with non-intersecting perpendicular axes.

3.3 Conclusions

In this paper algebraic screw pairs (A-pairs) and an algorithm for visualizing and comparing the reachable workspaces of short, dimensionally similar R- and A-chains has been presented. The algorithm is based on [11]. The ambient space around the manipulator is discretized into three dimensional pixel elements. Each joint angle is incremented in sequence by a small amount to determine which pixels are reached by the EE. The preliminary analysis indicates that the A-chains cannot precisely reproduce the reachable workspace of a geometrically similar R-chain with the

Table 3: DH-Parameters of the 2-jointed chains with non-intersecting perpendicular axes.

Chain/Link i	a_i	α_i	d_i	θ_{fi}	θ Range
2R-Chain					
1	0	-90°	8	N/A	$60^\circ \leq \theta_1 \leq 300^\circ$
2	5	0°	18	N/A	$-120^\circ \leq \theta_2 \leq 120^\circ$
2A-Chain					
1	0	90°	0	0°	$60^\circ \leq \theta_1 \leq 300^\circ$
2	5	0°	10	180°	$60^\circ \leq \theta_2 \leq 300^\circ$

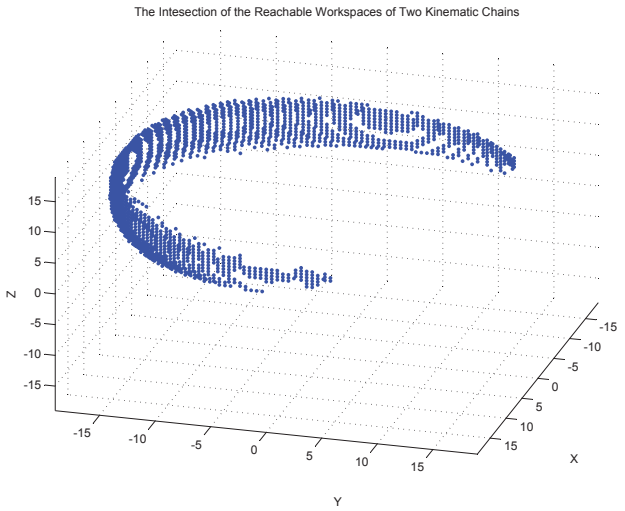

Figure 11: Plot of the intersection of the 2R-chain and 2A-chain reachable workspaces for 2-jointed chains with intersecting perpendicular axes.

same number of joints. However, the work presented here used A-pairs that were large relative to the size of the links, thereby exaggerating the difference between the two types of chains for illustrative purposes. In a real manipulator with appropriately sized joints the differences between the two workspaces would be much smaller.

The work thus far has involved directly comparing the ability of an A-chain to duplicate the displacements of an R-chain. Though an A-chain workspace may only match a small part of the R-chain workspace the A-chain workspace still has considerable size. A true measure of a manipulators usefulness is how it performs a desired task, not how well it matches an existing manipulator. Performance indices taking this into account will be considered in future research.

References

[1] J.D. Robinson. Direct and inverse kinematics of a new class of parallel-serial hybrid manipulator. Master's thesis, Carleton University, Canada, January 2008.

[2] M.L. Husty and A. Karger. Self-motions of Griffis-Duffy type parallel manipulators. In *Proceedings of ICRA '00 IEEE International Conference on Robotics and Automation*, pages 7–12, San Francisco, CA, USA, April 2000.

[3] H. Choset, K. Lynch, S. Hutchinson, G. Kantor, W. Burgard, L. Kavraki, and S. Thrun. *Principles of Robot Motion: Theory, Algorithms and Implementations*. The MIT Press, Cambridge, Massachusetts, 2005.

[4] B. Roth. Performance evaluation of manipulators from a kinematic viewpoint. *National Bureau of Standards, Special Publication*, (459):39–68, 1975.

[5] A. Kumar and K.J. Waldron. The dextrous workspace. ASME paper 80-DET-108, 1980.

[6] A. Kumar and K.J. Waldron. The workspaces of a mechanical manipulator. *ASME Journal of Mechanical Design*, 103(30):665–672, July 1981.

[7] D.C.H. Yang and T.W. Lee. On the workspace of mechanical manipulators. *ASME Journal of Mechanisms, Transmissions, and Automation in Design*, 105(1):62–69, 1983.

[8] T.W. Lee and D.H.C. Yang. On the evaluation of manipulator workspace. *ASME Journal of Mechanical Design*, 103(30):70–77, July 1981.

[9] Y.C. Tsai and A.H. Soni. An algorithm for the workspace of a general n-R robot. *ASME Journal of Mechanisms, Transmissions, and Automation in Design*, 105(1):52–57, 1983.

[10] A. Kumar and M.S. Patel. Mapping the manipulator workspace using interactive computer graphics. *The International Journal of Robotics Research*, 5(2):122–130, 1986.

[11] G. Castelli, E. Ottaviano, and M. Ceccarelli. A fairly general algorithm to evaluate workspace characteristics of serial and parallel manipulators. *Mechanics Based Design of Structures and Machines*, 36:14–33, 2008.

[12] J.D. Robinson. Preliminary analysis of the leg interference of a-pairs. Internal Progress Report, June 2008.